Critical review and experimental validation of radiative transfer models for semitransparent media containing large gas bubbles

Abhinav Bhanawat, Refet Ali Yalcin, Ricardo Martinez, Laurent Pilon *

Mechanical and Aerospace Engineering Department, Henry Samueli School of Engineering and Applied Science, University of California, Los Angeles, United States of America

ARTICLE INFO

ABSTRACT

Many materials manufacturing, photobiochemical, and photoelectrochemical processes involve radiation transfer through foams and bubbly fluids. Controlling and optimizing these processes require accurate predictions of radiation transfer through semitransparent media. Previously developed models treated the heterogeneous media as homogeneous plane-parallel slabs with some effective radiation characteristics while radiation transfer was governed by the one-dimensional radiative transfer equation (RTE). Unfortunately, their accuracy and range of validity remains unclear for lack of comparison with one another or against the same set of experimental data. This study aims to critically review and assess the validity of these models both numerically and experimentally. First, predictions of the transmittance and reflectance of heterogeneous slabs containing large randomly distributed bubbles were compared with those obtained from Monte Carlo ray-tracing (MCRT) method based on geometric optics. A new hybrid model was proposed that predicts the effective scattering coefficient and asymmetry factor using the Lorenz–Mie theory and the effective absorption coefficient as the volume-weighted sum of the bubbles and medium absorption coefficients and solves the RTE using the Monte Carlo method. Its predictions showed excellent agreement with those by the MCRT method for a wide range of bubble volume fractions (0%–30%) as well as slab thicknesses (2–40 mm) and medium absorption coefficients (0.1–100 m^{-1}). Second, microcomputed X-ray tomography scans were performed on a fused silica sample containing bubbles with mean radius of 480 μm to retrieve the exact locations, diameters, and total volume fraction of bubbles. Here also, predictions of the hybrid model using the retrieved data agreed well with experimental measurements of the spectral normal-hemispherical reflectance and transmittance of the sample for wavelengths between 0.4 and 3 μm when silica ranges from weakly absorbing to absorbing.

1. Introduction

Gas bubbles dispersed in a medium significantly change its thermophysical properties including its radiation characteristics [1]. In fact, bubbles substantially affect radiation transfer through a semitransparent medium by scattering the radiation and by increasing the absorption losses by lengthening the mean free path of photons [2]. For example, in glass manufacturing, gas bubbles are generated due to various chemical reactions taking place in the glassmelt [1,3]. The bubbles rise to the surface and may form a glass foam layer, reducing radiative heat transfer from the combustion space to the glassmelt [4,5], as illustrated in Fig. 1(a). Similarly, radiant barriers made by trapping air bubbles in a polymeric foam layer sandwiched between two layers of reflective foils are highly effective in minimizing radiative heat transfer from the roof of a building to the attic [6].

Solar water splitting involves generation of hydrogen or oxygen bubbles from semiconductor photoelectrodes immersed in an aqueous electrolyte, as depicted in Fig. 1(b) [7]. The bubbles scatter the incident sunlight and substantially decrease light absorption and photocurrent generation by the photoelectrode [7–12]. Likewise, bubbles injected into photobioreactors and raceway ponds for delivering carbon dioxide and stirring the microalgae suspension also scatter the sunlight strongly forward and enhance light penetration [13–15]. Similarly, air bubbles trapped in glass panes used in doors and windows give them a hazy appearance coveted for decorative and privacy purposes, as illustrated in Fig. 1(c).

Finally, light scattering by artificial seafoams covering the surface of oceans could potentially minimize absorption of the solar radiation by the Earth's surface by backscattering sunlight [16–18]. Indeed, seafoams are much more reflective than the bare ocean surface and thus appear white [see Fig. 1(d)] [16]. Given that oceans constitute nearly 71% of the Earth's surface, seafoams offer an efficient way of reducing the Earth's net heat input. However, concerns regarding the long-term

Nomenclature

$A_{n,\lambda}$	Spectral normal absorptance
C_{abs}	Absorption cross-section, mm^2
C_{sca}	Scattering cross-section, mm^2
f_v	Bubble volume fraction, %
g	Asymmetry factor
H	Thickness of glass slab, mm
I_λ	Spectral radiation intensity, Wsr^{-1} m^{-2} μm^{-1}
k	Absorption index
L	Length of square glass slab, mm
m	Complex refractive index, $m = n + ik$
n	Refractive index
Q_{abs}	Absorption efficiency factor
Q_{ext}	Extinction efficiency factor
Q_{sca}	Scattering efficiency factor
r	Bubble radius, mm
$\bar{r}$	Mean bubble radius, mm
$R_{nh,\lambda}$	Spectral normal-hemispherical reflectance
$T_{nh,\lambda}$	Spectral normal-hemispherical transmittance
y	Normalized absorption parameter
z	Location coordinate

Greek symbols

χ	Size parameter, $\chi = 2\pi r / \lambda$
κ_λ	Spectral absorption coefficient, m^{-1}
λ	Wavelength, μm
μ	Direction cosine, $\mu = \cos\theta$
Φ_λ	Spectral scattering phase function
ρ	Normalized size parameter
σ	Standard deviation
$\sigma_{s,\lambda}$	Spectral scattering coefficient, m^{-1}
θ	Scattering angle

Subscripts

a	Refers to air
d	Refers to dispersed phase (bubbles)
c	Refers to continuous medium (glass)
λ	Refers to spectral property

Superscript

tr	Refers to transport approximation

effects of ocean albedo manipulation on marine life and ecosystems remain [16]. Similarly, scattering of solar radiation by gas bubbles trapped in ice sheets could accelerate melting of ice during polar summers [19]. This is particularly important for ice-covered lakes, such as those in Tibetan plateau, where ice layers melt due to absorption of solar radiation by the ice enhanced by multiple scattering caused by entrapped gas bubbles [20,21].

It is often difficult to experimentally quantify the effect of bubbles on radiation transfer in the aforementioned situations owing to the complexity in characterizing the gas bubbles. Additionally, the effective radiation characteristics of a semitransparent medium containing gas bubbles cannot be predicted by the Lorenz–Mie theory since it is based on the assumption that the host medium is non-absorbing. This study aims to combine numerical, theoretical, and experimental methods to identify appropriate models capable of accurately predicting radiation

transfer through bubble-filled semitransparent slabs. First, the predictions of reflectance and transmittance by different models proposed in the literature were compared with those by the Monte Carlo ray-tracing method based on geometric optics for a large number of bubble volume fractions, slab thicknesses, and absorption coefficients of the continuous phase. Then, the models were experimentally validated by comparing their predictions with the measurements of the spectral normal-hemispherical reflectance and transmittance of a fused silica sample containing gas bubbles in the visible and near infrared. The results of this study could be instrumental in improving the design and performance of systems in the above mentioned applications.

2. Analysis

2.1. Problem statement

Let us consider an infinitely long and wide plane-parallel slab of semitransparent continuous medium of thickness H and spectral refractive $n_{c,\lambda}$ and absorption $k_{c,\lambda}$ indices, as illustrated in Fig. 2. The slab is surrounded by air ($n_{a,\lambda} = 1$) and contains randomly distributed polydisperse spherical and non-absorbing gas bubbles of refractive index $n_{d,\lambda} = 1.0$ occupying a volume fraction f_v and having normal size distribution $f(\bar{r}, \sigma)$ with mean radius $\bar{r}$ and standard deviation σ. The heterogeneous slab is subjected to collimated and normally incident radiation of wavelength λ. The bubbles are much larger than the wavelength λ so that geometric optics prevails while dependent scattering effects can be neglected due to the large interbubble distance compared with the wavelength [24]. The slab thickness and/or the bubble volume fraction are sufficiently large such that multiple scattering occurs. Bubbles scatter the radiation strongly forward such that a fraction of the incident intensity is transmitted through the slab in various directions, as quantified by the normal-hemispherical transmittance $T_{nh,\lambda}$. The remaining incident radiation is either backscattered, as accounted for by the normal-hemispherical reflectance $R_{nh,\lambda}$, or absorbed by the continuous phase, as represented by the absorptance $A_{n,\lambda}$. Overall, an energy balance on the incident radiation can be written as $R_{nh,\lambda} + A_{n,\lambda} + T_{nh,\lambda} = 1$.

3. Background

3.1. Monte Carlo ray-tracing method

Radiation transfer through a bubble-filled semitransparent medium can be simulated with high accuracy using the Monte Carlo ray-tracing (MCRT) method when geometric optics is valid [25,26]. The MCRT is a stochastic simulation method that traces millions of photon bundles or "rays" along their path in the computational domain as they undergo specular reflection or refraction at the bubble/medium or medium/surrounding interfaces according to Snell's law and Fresnel's equations [25].

The computational domain can be generated numerically by randomly distributing polydisperse bubbles in a semitransparent medium following an arbitrary size distribution. Alternatively, the location and size distribution of the bubbles can be experimentally determined by performing a microcomputed X-ray tomography (microCT) scan of an actual sample containing gas bubbles.

Finally, periodic boundary conditions (BCs) can be used to solve the one-dimensional radiative transfer equation for an infinite plane-parallel medium such that the rays reaching one edge of the computational domain re-enter the domain from the opposite edge maintaining their original direction. When the periodic BCs are eliminated, the rays reaching the edges of the medium undergo reflection/refraction at the medium/surrounding interface. The reflected rays are then traced on their onward path, while the refracted rays are considered as lost. Overall, each ray is traced until it is transmitted or reflected from the domain or absorbed in the semitransparent medium or lost from the
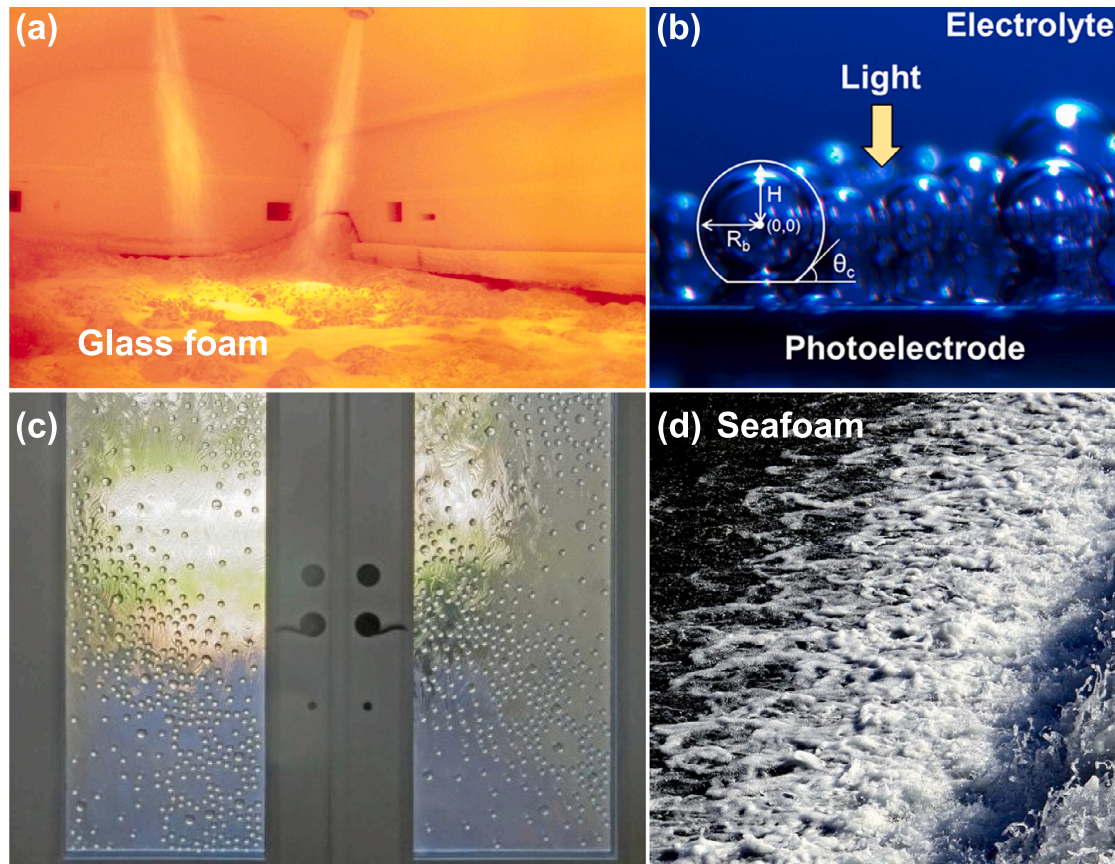
Fig. 1. Examples of bubbles in semitransparent media in various applications. (a) Foams in glass melting furnaces (credit: http://www.boconline.co.uk). (b) Gas bubbles generated during photoelectrochemical water splitting (reprinted with permission from Ref. [7]. Copyright © 2017 American Chemical Society). (c) Glass containing bubbles for decorative and privacy purposes in buildings [22]. (d) Seafoams generated to increase the ocean surface albedo and reduce solar absorption of Earth (credit: Stiller Beobachter [23]).
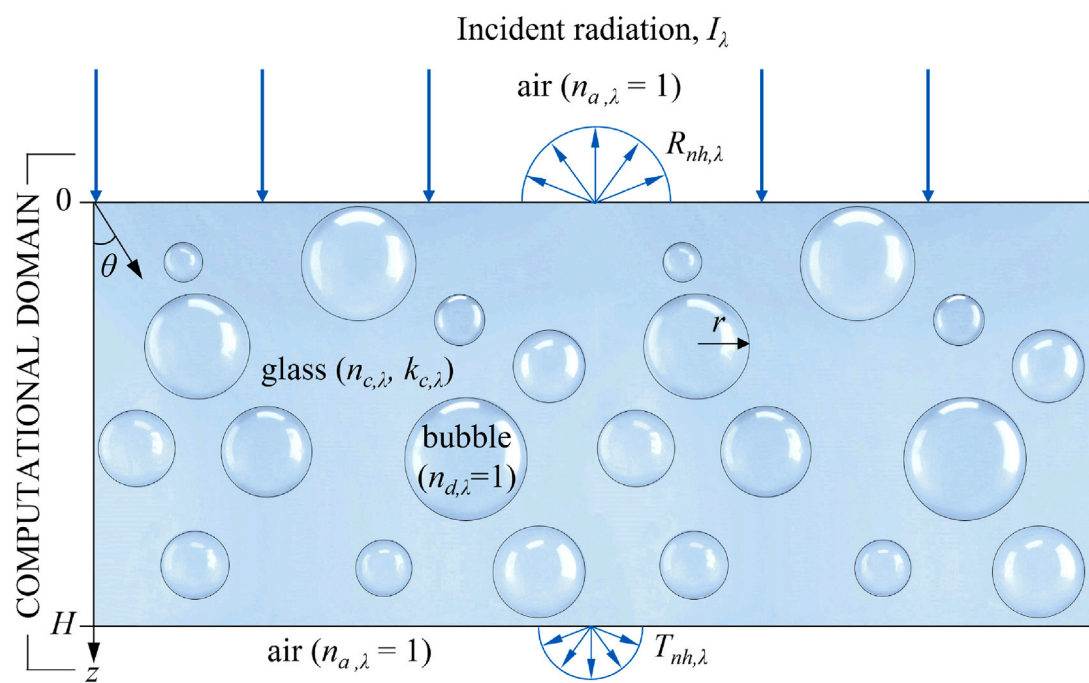

Fig. 2. Schematic of a plane-parallel slab of semitransparent medium ($n_{c,\lambda}$, $k_{c,\lambda}$) containing randomly distributed polydisperse spherical gas bubbles ($n_{d,\lambda} = 1$) and exposed to normally incident radiation.

edges. A sufficiently large number of rays (on the order of 10^6) is necessary to obtain numerically converged predictions of transmittance, reflectance, and absorptance [27,28]. In this study, predictions by the MCRT method will serve as a reference against which other models will be validated.

3.2. Homogeneous slabs with some effective properties

3.2.1. Radiative transfer equation

A less computationally intensive alternative to the MCRT method is to solve the radiative transfer equation (RTE) numerically. For an absorbing, scattering, and non-emitting medium, the one-dimensional steady-state RTE is expressed as [25]

$$\mu \frac{\partial I_\lambda(z,\theta)}{\partial z} = -(\kappa_\lambda + \sigma_{s,\lambda})I_\lambda(z,\theta) + \frac{\sigma_{s,\lambda}}{2}\int_{-1}^{1} I_\lambda(z,\theta')\Phi_\lambda(\theta',\theta)d\mu', \quad (1)$$

where $I_\lambda(z,\theta)$ is the spectral radiation intensity at location z and in direction $\mu = \cos\theta$, and the effective spectral radiation characteristics of the heterogeneous medium include the effective scattering coefficient $\sigma_{s,\lambda}$, the absorption coefficient κ_λ, and the effective scattering phase function $\Phi_\lambda(\theta',\theta)$. The latter corresponds to the probability of a photon incident from direction $\mu' = \cos\theta'$ being scattered in the direction of interest $\mu = \cos\theta$. Conventionally, these effective radiation characteristics are determined based on the superposition principle for an ensemble of bubbles, assuming the bubbles scatter independently of each other. Most studies investigating radiation transfer through absorbing media containing spherical particles (or bubbles) have modeled them as homogeneous with some effective radiation characteristics κ_λ, $\sigma_{s,\lambda}$, and $\Phi_\lambda(\theta',\theta)$ assuming independent scattering [29–39], as reviewed in the next sections.

3.2.2. Fedorov-Viskanta model

Fedorov and Viskanta [34,35] developed a theoretical framework for predicting radiation transfer through glass foams consisting of monodisperse bubbles of radius r with volume fraction $f_v \le 0.74$. First, the effective scattering $\sigma_{s,\lambda}$ and absorption κ_λ coefficients of a layer of foams made of monodisperse bubbles were based on the anomalous diffraction theory and given by [40]

$$\sigma_{s,\lambda} = 0.75 Q^d_{sca,\lambda}\frac{f_v}{r} \quad \text{and} \quad \kappa_\lambda = \frac{4\pi k_{c,\lambda}}{\lambda} - 0.75(Q^c_{abs,\lambda} - Q^d_{abs,\lambda})\frac{f_v}{r}. \quad (2)$$

The expression of the effective absorption coefficient κ_λ was obtained by subtracting the absorption coefficient of spherical glass particles in air from that of a glass slab and adding the absorption coefficient of spherical gas bubbles in glass using their respective absorption efficiency factors $Q^c_{abs,\lambda}$ and $Q^d_{abs,\lambda}$ given by [40]

$$Q^d_{abs,\lambda} = 1 + \frac{e^{-2\rho_{d,\lambda}\tan(y_{d,\lambda})}}{\rho_{d,\lambda}\tan(y_{d,\lambda})} + \frac{e^{-2\rho_{d,\lambda}\tan(y_{d,\lambda})}-1}{2[\rho_{d,\lambda}\tan(y_{d,\lambda})]^2}, \quad (3)$$

$$Q^c_{abs,\lambda} = 1 + \frac{e^{-2\rho_{c,\lambda}\tan(y_{c,\lambda})}}{\rho_{c,\lambda}\tan(y_{c,\lambda})} + \frac{e^{-2\rho_{c,\lambda}\tan(y_{c,\lambda})}-1}{2[\rho_{c,\lambda}\tan(y_{c,\lambda})]^2}, \quad (4)$$

where $\rho_{d,\lambda}$ and $\rho_{c,\lambda}$ are the Van de Hulst's normalized size parameters defined as [40]

$$\rho_{d,\lambda} = \frac{4(n_{d,\lambda}-1)\pi r}{\lambda} \quad \text{and} \quad \rho_{c,\lambda} = \frac{4(n_{c,\lambda}-1)\pi r}{\lambda}. \quad (5)$$

The corresponding normalized absorption parameters y_d and y_c were given by [40]

$$y_{d,\lambda} = \tan^{-1}\left(\frac{k_{d,\lambda}}{n_{d,\lambda}-1}\right) \quad \text{and} \quad y_{c,\lambda} = \tan^{-1}\left(\frac{k_{c,\lambda}}{n_{c,\lambda}-1}\right). \quad (6)$$

Additionally, the extinction efficiency factor $Q^d_{ext,\lambda}$ of a bubble in glass was expressed by [40]

$$Q^d_{ext,\lambda} = 2 - 4\frac{\cos(y_{d,\lambda})}{\rho_{d,\lambda}}\left[e^{-\rho_{d,\lambda}\tan(y_{d,\lambda})}\sin(\rho_{d,\lambda}-y_{d,\lambda})\right]$$
$$+ 4\left[\frac{\cos(y_{d,\lambda})}{\rho_{d,\lambda}}\right]^2\left[\cos(2y_{d,\lambda}) - e^{-\rho_{d,\lambda}\tan(y_{d,\lambda})}\cos(\rho_{d,\lambda}-2y_{d,\lambda})\right]. \quad (7)$$

The corresponding scattering efficiency factor of a bubble in glass $Q^d_{sca,\lambda}$ was written as

$$Q^d_{sca,\lambda} = Q^d_{ext,\lambda} - Q^d_{abs,\lambda}. \quad (8)$$

Finally, the RTE was solved using the two-flux approximation method to obtain closed form analytical expressions for the normal-hemispherical transmittance $T_{nh,\lambda}$, reflectance $R_{nh,\lambda}$, and absorptance $A_{n,\lambda}$ of an absorbing and scattering glass slab containing bubbles. The model assumed isotropic radiation field inside the glass slab owing to the large bubble volume fraction. Therefore, the model calculated the reflectance at the glass slab/air interface using a correlation applicable for any diffuse media-to-air interface [41,42]. The reflectance at air/glass slab interface was calculated using Fresnel's equation [25]. In the present study, the glass slabs containing gas bubbles were free-standing with air on both sides and the interface reflectances were calculated accordingly.

3.2.3. Dombrovsky model

Dombrovsky et al. [36,37] used Lorenz–Mie theory to calculate the spectral transport scattering $Q^{tr}_{sca,\lambda}$ and absorption $Q_{abs,\lambda}$ efficiency factors of large bubbles of size parameter $\chi_d = 2\pi r/\lambda$ embedded in a semitransparent medium of complex refractive index $m_{c,\lambda} = n_{c,\lambda} + ik_{c,\lambda}$ given by

$$Q^{tr}_{sca,\lambda} = 0.9(n_{c,\lambda}-1) \quad \text{and} \quad Q_{abs,\lambda} = -\frac{8}{3}k_{c,\lambda}\chi_d. \quad (9)$$

The effective scattering $\sigma_{s,\lambda}$, transport scattering $\sigma^{tr}_{s,\lambda}$, and absorption κ_λ coefficients of the heterogeneous medium were given by [36]

$$\sigma_{s,\lambda} = \frac{3f_v}{2r}, \quad \sigma^{tr}_{s,\lambda} = 0.675(n_{c,\lambda}-1)\frac{f_v}{r}, \quad \text{and} \quad \kappa_\lambda = (1-f_v)\kappa_{c,\lambda} \quad (10)$$

where $\kappa_{c,\lambda} = 4\pi k_{c,\lambda}/\lambda$ is the absorption coefficient of the continuous semitransparent medium. In addition, the authors used the so-called "transport approximation" to simplify the radiative transfer equation by replacing the scattering phase function by a sum of the isotropic component and the term denoting the peak of forward scattering given by [43,44]

$$\Phi^{tr}_\lambda(\theta_\circ) = 1 - g_\lambda + 2g_\lambda\delta(1-\cos\theta_\circ), \quad (11)$$

where δ is the Kronecker-delta function, $\theta_\circ$ is the angle between the radiation incident on the scatterer along direction $\mu' = \cos\theta'$ and the intensity scattered in direction $\mu = \cos\theta$. The asymmetry factor g_λ was given by [36]

$$g_\lambda = 1 - 0.45(n_{c,\lambda}-1). \quad (12)$$

The RTE was then solved using the modified two-flux approximation method accounting for boundary reflections at the surfaces of the plane-parallel slab surrounded by air. Analytical expressions for $T_{nh,\lambda}$ and $R_{nh,\lambda}$ were derived. The authors reported an error of less than 5% when compared with the numerical calculations based on the composite discrete ordinate method for the range of size parameter $20 \ll \chi_d \ll 1/(2k_{c,\lambda})$.

3.2.4. Modified Lorenz–Mie theory

Yang et al. [38] established that the scattering and extinction efficiencies of a spherical particle embedded in an absorbing medium presented by Sudiarta et al. [31] and Fu et al. [32] were inherent properties derived from the near-field at the particle surface. Yang et al. [38] further noted that the corresponding scattering and extinction cross-sections could not be calculated by multiplying these efficiencies with the geometric projected area of the spherical particle since the host medium was absorbing. Therefore, the authors derived the expressions for apparent scattering and absorption cross-sections based on the far-field information to determine the effective radiation characteristics [38]. The apparent scattering cross-section was scaled by a factor $\exp(\kappa_{c,\lambda}r)$ to facilitate radiative transfer calculations involving
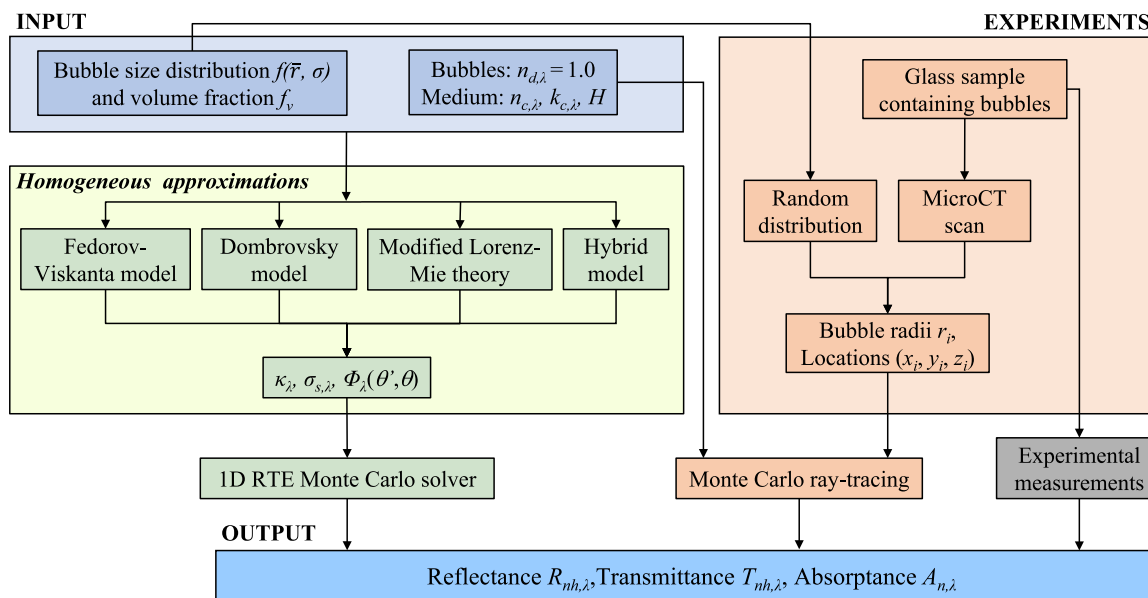
Fig. 3. Different numerical, theoretical, and experimental approaches to determine the spectral normal-hemispherical reflectance $R_{nh,\lambda}$, transmittance $T_{nh,\lambda}$, and absorptance $A_{n,\lambda}$ of semitransparent media containing gas bubbles.

a polydisperse particle system. This scaled apparent scattering cross-section was used to determine the effective scattering coefficient $\sigma_{s,\lambda}$ of a semitransparent glass slab containing gas bubbles. The corresponding effective absorption coefficient κ_λ was equal to the absorption coefficient of glass $\kappa_{c,\lambda}$ regardless of the volume fraction f_v of bubbles [38]. The asymmetry parameter g_λ was the same as that predicted by Lorenz–Mie theory for bubbles in a non-absorbing medium. These radiation characteristics were input into a 1D RTE solver based on the Monte Carlo ray-tracing method to calculate the normal-hemispherical reflectance R_{nh} and transmittance T_{nh} while also accounting for boundary reflections at air/glass slab interfaces.

3.2.5. Hybrid model

Here, we propose a hybrid model in which (i) the effective scattering coefficient $\sigma_{s,\lambda}$ and asymmetry factor g_λ of the heterogeneous medium were predicted by the Lorenz–Mie theory assuming the continuous medium was non-absorbing and (ii) the effective absorption coefficient κ_λ was expressed as a weighted sum of the absorption coefficients of the dispersed and continuous phases as used in the literature [36,45]

$$\kappa_\lambda = (1 - f_v)\kappa_{c,\lambda}. \tag{13}$$

The Henyey–Greenstein phase function was used to model the scattering phase function using the asymmetry parameter g_λ. Yalcin et al. [46] developed a code available online [47] that computes these radiation characteristics and predicts the normal-hemispherical reflectance R_{nh} and transmittance T_{nh} by solving the one-dimensional RTE [Eq. (1)] using the Monte Carlo method. The code also accounts for reflection and refraction at the boundaries of the plane-parallel heterogeneous slab. Typically, about 10^6 rays are necessary to achieve numerical convergence.

The objective of the study is to assess the validity of the above theoretical models for simulating radiation transfer in semitransparent media containing large gas bubbles. To do so, predictions of the effective radiation characteristics κ_λ, $\sigma_{s,\lambda}$, and $\Phi_\lambda(\theta',\theta)$ as well as the normal-hemispherical reflectance $R_{nh\lambda}$ and transmittance $T_{nh\lambda}$ by the different models were compared with those by the Monte Carlo ray-tracing method based on geometric optics. Furthermore, experimental measurements of the spectral normal-hemispherical reflectance $R_{nh\lambda}$ and transmittance $T_{nh\lambda}$ of a thick fused silica sample containing bubbles between 0.4 and 3 μm were compared with predictions by the different

models as well as by the Monte Carlo ray-tracing method for the sample's digital twin generated from microcomputed X-ray tomography (microCT) scans.

4. Materials and methods

4.1. Glass sample containing bubbles

A glass sample made of Osram Sylvania SG25 Lightning grade fused silica and containing gas bubbles was analyzed [48]. The sample was cut with a diamond saw from a large piece of fused silica collected during shutdown of a glass melting furnace [48]. The sample had a thickness of 10 mm and a 43 mm × 38 mm cross-section. The gas bubbles were spherical and appeared to be randomly distributed in the sample. The optical properties ($n_{c,\lambda}$, $k_{c,\lambda}$) of fused silica were obtained from Refs. [48–50].

4.2. Bubble characterization

To characterize the bubbles present in the glass sample, microCT scans were performed on the CrumpCAT scanner at UCLA Crump Institute of Molecular Imaging having a resolution of 125 μm. The scans achieved excellent contrast between the bubbles and the glass [see flythrough video in Supplementary Material] which allowed them to be easily distinguished during post-processing. The scans also confirmed that the bubbles were spherical owing to the high surface tension of glassmelt. Any conjoined bubbles were separated by fitting two separate spheres. The diameter and coordinates of each bubble were extracted from the tomographic data using the open-source medical imaging data analysis software AMIDE [51]. The normal size distribution $f(\bar{r},\sigma)$ was fitted to be used in the radiation transfer models previously described.

4.3. Reflectance and transmittance measurements

A double-beam ultraviolet–visible (UV–Vis) spectrophotometer (Evolution[TM] 220, Thermo Scientific Fisher, USA) equipped with an integrating sphere (Evolution[TM] ISA-200 Integrating Sphere Accessory, Thermo Scientific Fisher, USA) was used for measuring the normal-hemispherical reflectance $R_{nh,\lambda}$ and transmittance $T_{nh,\lambda}$ of the glass sample containing bubbles over the wavelength range 0.4 to 1 μm
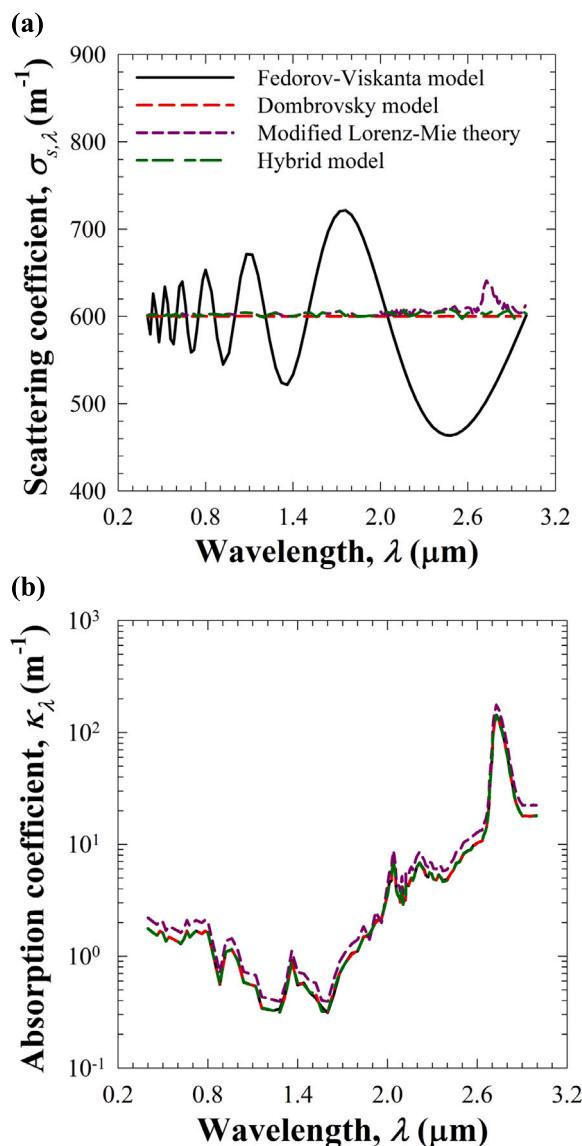
(a)

(b)

Fig. 4. Comparison of the effective spectral (a) scattering $\sigma_{s,\lambda}$ and (b) absorption κ_λ coefficients predicted by four different models as functions of the wavelength of incident radiation for monodisperse bubbles of radius $r = 0.5$ mm and volume fraction $f_v = 20\%$.

when glass is transparent. The diameter of the spectrophotometer beam was relatively small compared to the sample dimensions (43 mm × 38 mm). Therefore, measurements were taken at 10 different locations over the sample surface to correct for local variations in bubble volume fraction. A similar procedure was repeated for the measurements of reflectance $R_{nh,\lambda}$ and transmittance $T_{nh,\lambda}$ over the 2 to 3 μm spectral range when glass is absorbing. The measurements were performed on a nitrogen-purged Fourier transform infrared (FTIR) spectrometer (Nicolet^{TM} iS50, Thermo Scientific Fischer, USA) equipped with an MCT detector and a KBr beamsplitter, along with an integrating sphere (Upward IntegratIR^{TM}, PIKE Technologies, USA).

5. Results and discussion

5.1. Introduction

Fig. 3 shows a flowchart detailing the different methods and models used in this study to predict the spectral normal-hemispherical reflectance $R_{nh,\lambda}$, transmittance $T_{nh,\lambda}$, and absorptance $A_{n,\lambda}$ of a fused

silica glass slab containing bubbles. The bubbles were non-absorbing and had a refractive index $n_{d,\lambda} = 1.0$, volume fraction f_v, and size distribution $f(\bar{r}, \sigma)$. Predictions by the different models were evaluated against those by the Monte Carlo ray-tracing method, as previously described.

5.2. Effective radiation characteristics

Fig. 4 compares the effective spectral (a) scattering $\sigma_{s,\lambda}$ and (b) absorption κ_λ coefficients as functions of wavelength λ as predicted by the four different models for monodisperse bubbles of radius $r = 0.5$ mm and volume fraction $f_v = 20\%$. Fig. 4(a) shows that the effective scattering coefficient $\sigma_{s,\lambda}$ predicted by the hybrid model and by the Dombrovsky model [see Eq. (10)] remained nearly constant over the spectral range considered. This can be attributed to the large size parameter that caused the scattering and extinction efficiency factors $Q_{ext}^d = Q_{sca}^d$ to reach a value of 2 [25]. The predictions of $\sigma_{s,\lambda}$ by the modified Lorenz–Mie theory agreed well with those by the Lorenz–Mie theory. However, the predicted scattering coefficient $\sigma_{s,\lambda}$ exhibited a peak when absorption by the host medium peaked at around $\lambda = 2.73$ μm. Such a behavior seems erroneous and may be attributed to the large bubble radius r that increased the magnitude of the exponential scaling factor $\exp(\kappa_{c,\lambda} r)$ used in the modified Lorenz–Mie theory model. On the other hand, the effective scattering coefficient predicted by the Fedorov–Viskanta model oscillated around the predictions by the Lorenz–Mie theory. Such oscillations can be attributed to wave effects captured by the anomalous diffraction theory [40].

Fig. 4(b) shows that predictions of the effective absorption coefficients κ_λ by the hybrid model, the Dombrovsky model, and the Fedorov–Viskanta model were all in agreement. However, predictions by the modified Lorenz–Mie theory were uniformly larger than the other models by 25% at all wavelengths since it considered $\kappa_\lambda = \kappa_{c,\lambda}$ instead of $\kappa_\lambda = \kappa_{c,\lambda}(1 - f_v)$. Fig. 4(b) also highlights that the medium was weakly absorbing up to $\lambda = 2$ μm. Beyond that wavelength, the absorption of the medium consistently increased, exhibiting an absorption peak at about $\lambda = 2.73$ μm.

5.3. Effect of volume fraction f_v

Fig. 5 compares the normal-hemispherical (a) reflectance $R_{nh,\lambda}$ and (b) transmittance $T_{nh,\lambda}$ predicted as functions of bubble volume fraction f_v by the four different models for monodisperse bubbles of radius $r = 0.5$ mm, slab thickness $H = 10$ mm, and wavelength $\lambda = 2$ μm when the medium was weakly absorbing ($k_{c,\lambda} = 7.3 \times 10^{-7}$). Similarly, Fig. 5(c) and 5(d) respectively present the normal-hemispherical reflectance $R_{nh,\lambda}$ and transmittance $T_{nh,\lambda}$ but at wavelength $\lambda = 2.73$ μm when the medium was significantly more absorbing ($k_{c,\lambda} = 3.27 \times 10^{-5}$). Fig. 5 shows that all the models predicted a similar trend of increasing reflectance $R_{nh,\lambda}$ and decreasing transmittance $T_{nh,\lambda}$ with increasing bubble volume fraction f_v for both wavelengths considered. It also shows that the Fedorov–Viskanta model consistently overpredicted the reflectance $R_{nh,\lambda}$ and underestimated the transmittance $T_{nh,\lambda}$ for all volume fractions considered. This can be attributed to the fact that the Fedorov–Viskanta model assumed isotropic radiation field inside the medium to calculate the reflectance of medium/air interface [34]. Such an assumption is valid for foams that have bubble volume fraction $f_v \sim 74\%$ but may not be realistic for smaller f_v. Interestingly, the predictions by the Dombrovsky model were in agreement with those by the MCRT method at wavelength $\lambda = 2$ μm when fused silica was weakly absorbing. However, the model overestimated considerably the transmittance $T_{nh,\lambda}$ as well as the reflectance $R_{nh,\lambda}$ at $\lambda = 2.73$ μm when fused silica was more absorbing. Similarly, the predictions of reflectance $R_{nh,\lambda}$ and transmittance $T_{nh,\lambda}$ by the modified Lorenz–Mie theory agreed well with those by the MCRT method for a weakly absorbing glass medium at wavelength $\lambda = 2$ μm. However, when the medium was more absorbing at $\lambda = 2.73$ μm, the predictions of
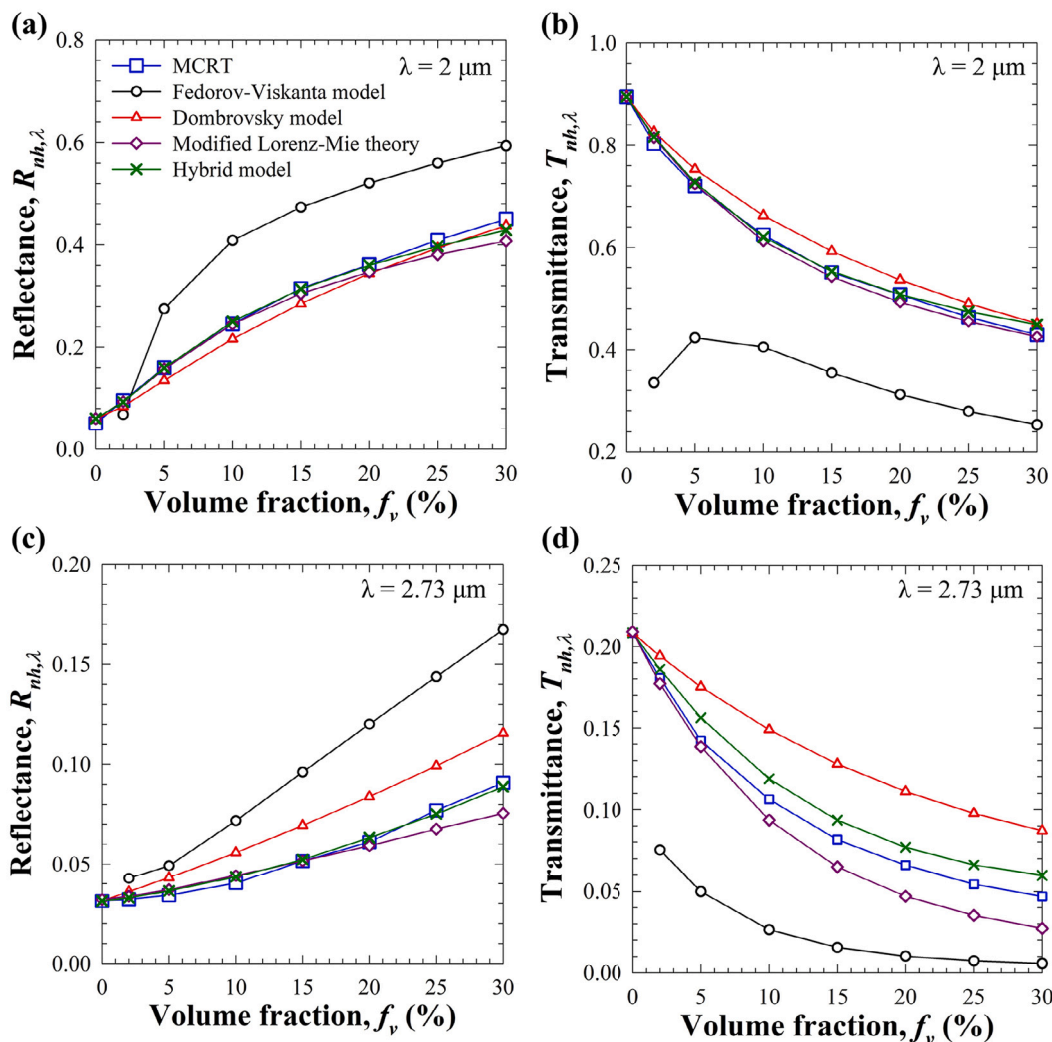
Fig. 5. Comparison of predictions of the normal-hemispherical reflectance $R_{nh,\lambda}$ and transmittance $T_{nh,\lambda}$ as functions of bubble volume fraction f_v for (a)–(b) wavelength $\lambda = 2$ μm when fused silica was weakly absorbing and (c)–(d) at $\lambda = 2.73$ μm when fused silica was more absorbing. The bubbles were monodisperse with radius $r = 0.5$ mm and the slab's thickness was $H = 10$ mm. Predictions by the MCRT method are used as reference.

transmittance $T_{nh,\lambda}$ were slightly smaller than those predicted by the MCRT method. This deviation can also be attributed to the fact that the modified Lorenz–Mie theory did not take into account the bubble volume fraction f_v for predicting the effective absorption coefficient κ_λ of the glass slab containing bubbles, as previously discussed. Finally, Fig. 5 establishes that the predictions of $R_{nh,\lambda}$ and $T_{nh,\lambda}$ by the hybrid model were in excellent agreement with those by the MCRT method for all volume fractions and for both wavelengths considered.

5.4. Effect of continuous phase absorption coefficient $\kappa_{c,\lambda}$

Fig. 6 compares the predictions of the normal-hemispherical (a) re-flectance $R_{nh,\lambda}$ and (b) transmittance $T_{nh,\lambda}$ by the four different models against predictions by the MCRT method as functions of the absorption coefficient $\kappa_{c,\lambda}$ of the continuous phase for monodisperse bubbles of radius $r = 0.5$ mm and volume fraction $f_v = 20\%$ in a slab of thickness $H = 10$ mm. Here again, the Fedorov–Viskanta model overestimated the reflectance $R_{nh,\lambda}$ and underestimated the transmittance $T_{nh,\lambda}$ as compared with predictions by the MCRT method. The Dombrovsky model slightly overestimated the transmittance $T_{nh,\lambda}$ by an absolute error of about 6% while the predicted reflectance $R_{nh,\lambda}$ fell within an absolute difference of 5% of that predicted by the MCRT method for all absorption coefficients $\kappa_{c,\lambda}$ considered. The predictions of $R_{nh,\lambda}$ and

$T_{nh,\lambda}$ by the modified Lorenz–Mie theory agreed well with those by the MCRT method for small absorption coefficients such that $\kappa_{c,\lambda} \leq 5$ m^{-1}. However, for larger absorption coefficients, the predicted transmittance $T_{nh,\lambda}$ was slightly smaller than that predicted by the MCRT method. On the other hand, the hybrid model accurately predicted the reflectance $R_{nh,\lambda}$ and transmittance $T_{nh,\lambda}$ for the range of absorption coefficients $\kappa_{c,\lambda}$ between 10^{-1} to around 10^2. This model was able to accurately predict radiation transfer in a semitransparent medium containing bubbles when absorption was negligible and scattering dominated, and also when absorption dominated and scattering was negligible. In the latter case, potential errors made in predicting the effective scattering coefficient $\sigma_{s,\lambda}$ had no effect in the predictions of $R_{nh,\lambda}$ and $T_{nh,\lambda}$.

5.5. Effect of slab thickness H

Fig. 7 compares the normal-hemispherical (a) reflectance $R_{nh,\lambda}$ and (b) transmittance $T_{nh,\lambda}$ predicted by the four different models as func-tions of the slab's thickness H for monodisperse bubbles of radius $r = 0.5$ mm and volume fraction $f_v = 20\%$ at wavelength $\lambda = 2$ μm. Here again, the Fedorov–Viskanta model overestimated $R_{nh,\lambda}$ and underestimated $T_{nh,\lambda}$ for all thicknesses H considered except for $H < 5$ mm. In addition, the Dombrovsky model slightly underestimated the reflectance $R_{nh,\lambda}$ for thickness $H < 15$ mm but overpredicted it
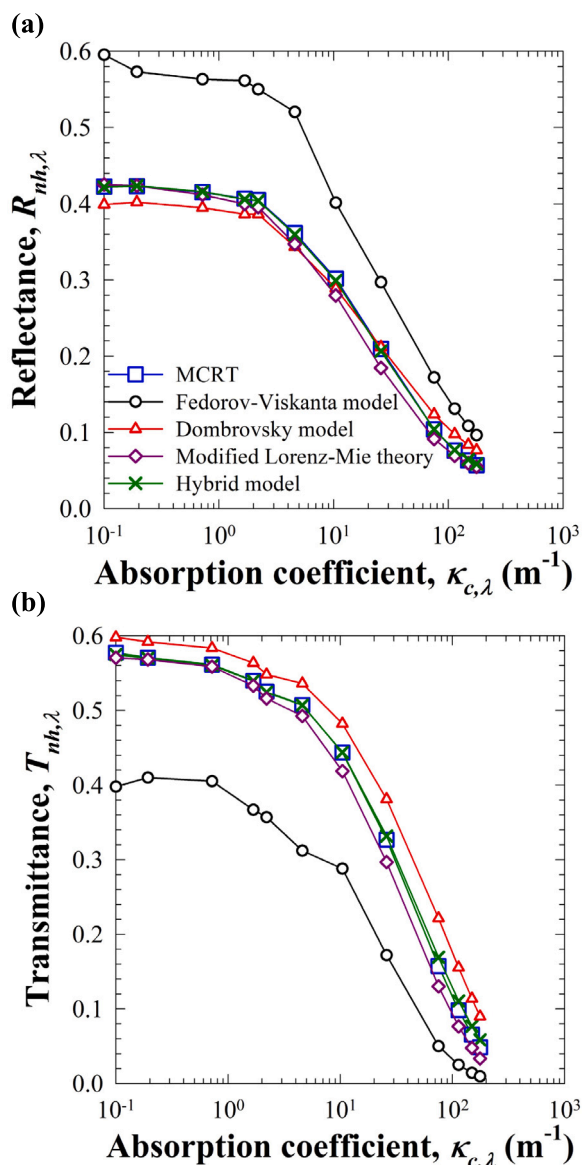
Fig. 6. Comparison of predictions of the normal-hemispherical (a) reflectance $R_{nh,\lambda}$ and (b) transmittance $T_{nh,\lambda}$ as functions of continuous phase absorption coefficient $\kappa_{c,\lambda}$. The bubbles were monodisperse with radius $r = 0.5$ mm and volume fraction $f_v = 20\%$ while the slab's thickness was $H = 10$ mm.

Fig. 7. Comparison of predictions of the normal-hemispherical (a) reflectance $R_{nh,\lambda}$ and (b) transmittance $T_{nh,\lambda}$ as functions of slab's thickness H for monodisperse bubbles of radius $r = 0.5$ mm and volume fraction $f_v = 20\%$ at wavelength $\lambda = 2$ μm.

as the thickness increased. However, its predictions of transmittance $T_{nh,\lambda}$ agreed reasonably well with the predictions by the MCRT method for all thicknesses. Similarly, the modified Lorenz–Mie theory slightly underestimated the reflectance $R_{nh,\lambda}$ and transmittance $T_{nh,\lambda}$ as the slab thickness increased due to its overestimation of the effective absorption coefficient κ_λ. Finally, the reflectance $R_{nh,\lambda}$ and transmittance $T_{nh,\lambda}$ predicted by the hybrid model were in excellent agreement with those predicted by the MCRT method even for sample thicknesses on the same order of magnitude as the bubble radius. This may seem surprising because defining effective radiation characteristics may not be valid for such small thicknesses given the few bubbles interacting with the incident light. However, the simulated samples had infinite cross-sectional area thanks to the periodic boundary conditions. Thus, averaging was achieved over a large surface area. Similar considerations were made experimentally by using a wide beam compared with the sample thickness [48].
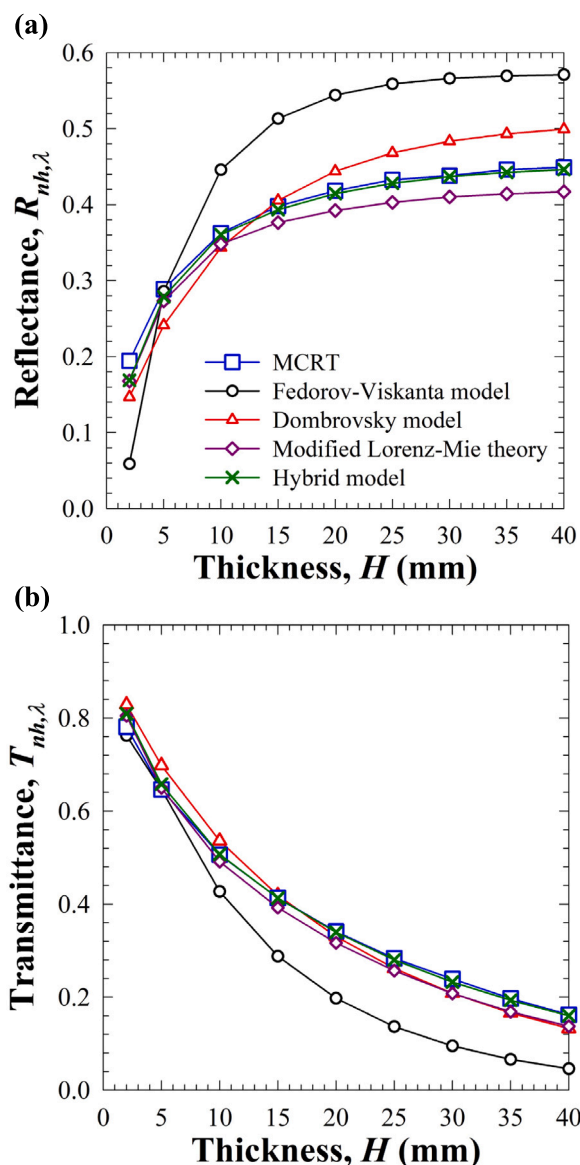
5.6. Comparison with experimental measurements

5.6.1. Bubble characterization

Fig. 8 shows (a) the photograph of the sample's top view with (b) the corresponding image of the sample's digital twin created from microCT scans, indicating an excellent 3D reconstruction. Fig. 8(c) shows a screenshot from the user interface of imaging software AMIDE, highlighting the identified bubbles in the sample at a depth of 7 mm from the top of the sample. Finally, Fig. 8(d) shows the retrieved bubble size distribution from the 636 bubbles contained in the sample with the best fit provided by a normal distribution with a mean bubble radius $\bar{r} = 0.48$ mm and standard deviation $\sigma = 0.12$ mm. The total bubble volume fraction f_v in the sample was determined to be 2%.

The sample was sufficiently thick and the bubble volume fraction large enough for multiple scattering to prevail. Thus, the selected sample and the selected wavelength range captured different light transfer phenomena such as absorption and multiple scattering. However, retrieving the location and size distribution of the bubbles was
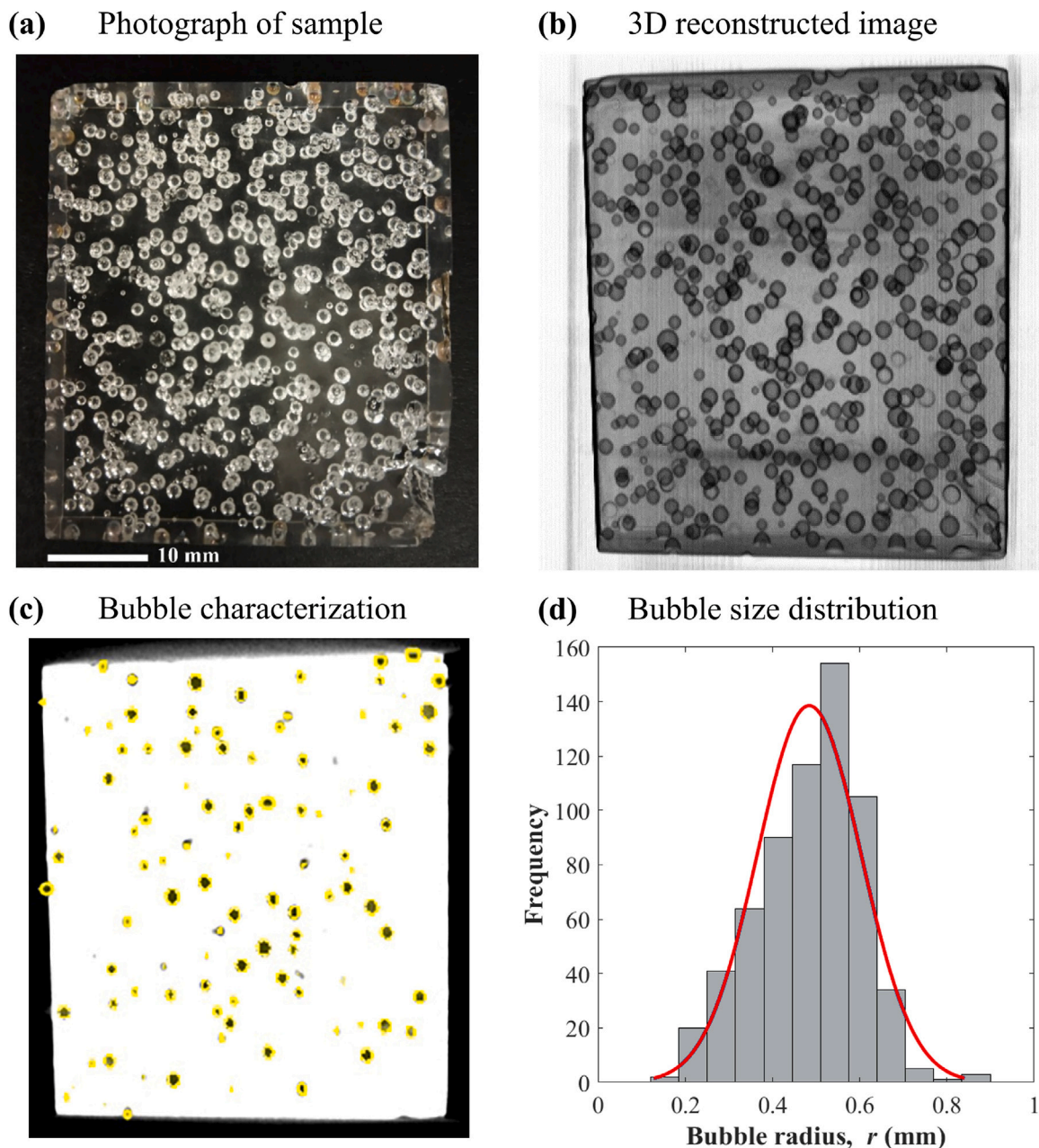
(a)　　Photograph of sample

(b)　　3D reconstructed image

(c)　　Bubble characterization

(d)　　Bubble size distribution

Fig. 8. (a) Photograph of the glass sample containing gas bubbles and (b) its 3D reconstructed image obtained from microcomputed X-ray tomography. (c) The radius and location of each bubble was identified using medical imaging software AMIDE. (d) Retrieved bubble size distribution fitted with a normal distribution $f(\bar{r}, \sigma)$ with mean bubble radius $\bar{r} = 0.48$ mm and standard deviation $\sigma = 0.12$ mm.

challenging because the microCT scans had multiple slices containing portions of the same bubble which prevented the use of image processing programs that use Hough circle transform to quickly extract circular objects from a single slice. Instead, medical imaging tools that can identify and characterize volumes from microCT scans were necessary. However, most open source medical imaging tools did not automatically detect the volumes and required manual identification which was challenging and tedious when dealing with a large number of scattering bubbles.

5.6.2. Normal-hemispherical reflectance and transmittance

Fig. 9 compares the experimental measurements of the normal-hemispherical (a) reflectance $R_{nh,\lambda}$ and (b) transmittance $T_{nh,\lambda}$ over the wavelength range $\lambda = 0.4$–1 μm when the glass was weakly absorbing with those predicted numerically by the MCRT method using the specific locations and radii of the bubbles extracted from microCT

scan. Similarly, Fig. 9(c) and 9(d) present the corresponding results over the wavelength range $\lambda = 2$–3 μm when the glass was absorbing. Note that the reported experimental measurements for the glass sample covered a wide range of glass absorption coefficients. The experimental measurements had a small relative error of around 2% and the error bands are shown in gray. The predictions by the hybrid model using the bubble size distribution reported in Fig. 8(d) for volume fraction $f_v = 2\%$ are also presented. In addition, the results for the case without bubbles (i.e., $f_v = 0\%$) are provided as a reference. Here again, the predictions by the hybrid model combined with 1D Monte carlo simulations agreed very well with predictions by the MCRT model using periodic boundary conditions. The absolute differences of about 6%–7% in the reflectance $R_{nh,\lambda}$ and of about 3%–4% in the transmittance $T_{nh,\lambda}$ predicted by the hybrid model and experimental measurements were most likely due to radiation losses through the edges of the sample after scattering by bubbles. This is confirmed by the predictions by
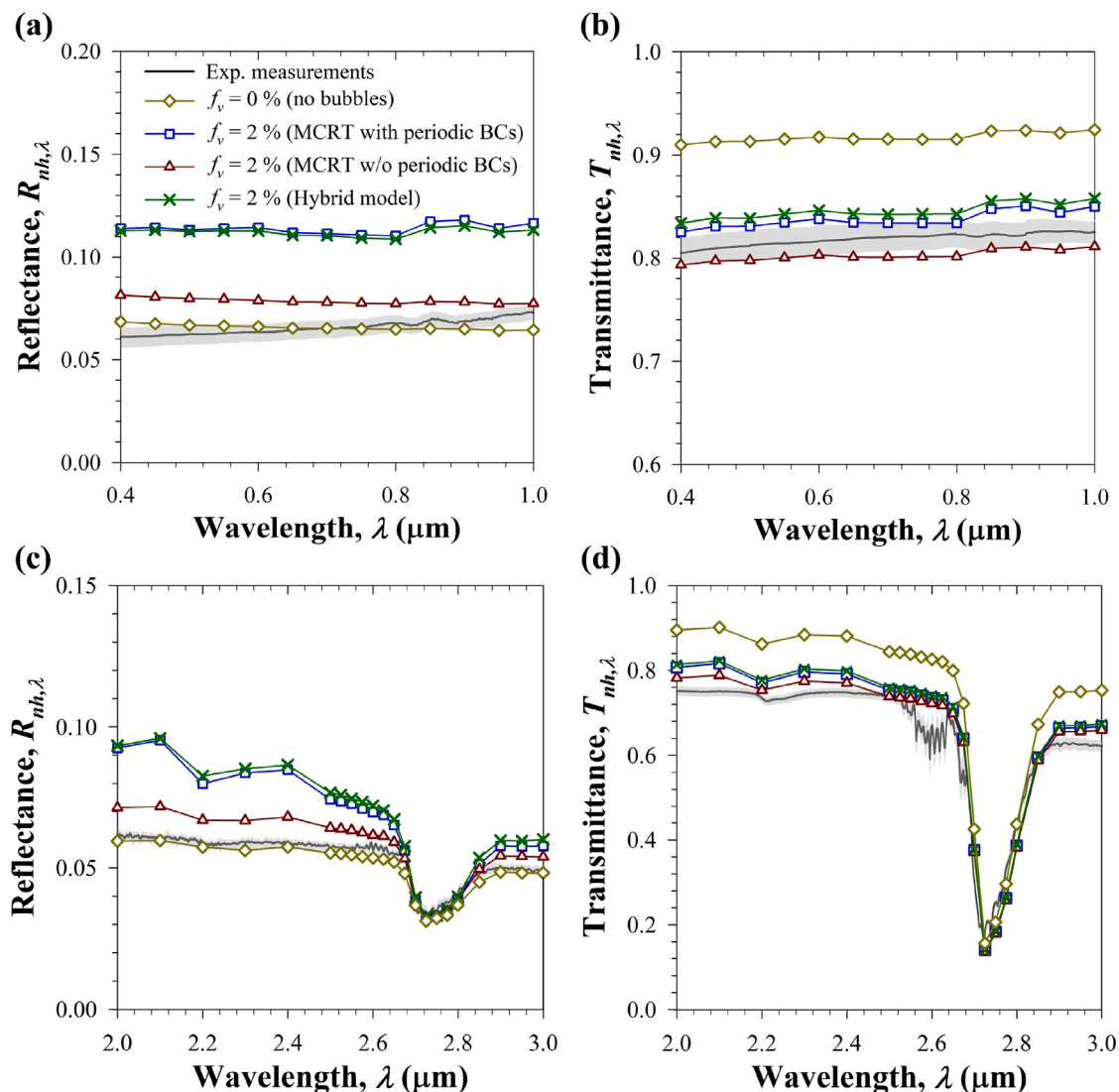
Fig. 9. Comparison of the experimentally measured spectral normal-hemispherical reflectance $R_{nh,\lambda}$ and transmittance $T_{nh,\lambda}$ as functions of wavelength λ with the predictions by Monte Carlo ray-tracing method with and without periodic boundary conditions for wavelength range (a–b) $\lambda = 0.4–1$ μm and (c–d) $\lambda = 2–3$ μm. Predictions for the case without bubbles ($f_v = 0\%$) are also provided as a reference.

the MCRT method without periodic boundary conditions (BCs) which agree better with the experimental measurements across the spectral range considered. In addition, the trends in the spectral variations of the predicted reflectance and transmittance differ slightly from their experimental measurements. This was most likely due to differences between the actual optical properties of the glass sample and those used in the simulations and obtained from the literature for fused silica [49,50].

6. Conclusion

This study combined experimental, numerical, and theoretical methods to assess the validity of three previously proposed models predicting radiation transfer through semitransparent slabs containing large non-absorbing gas bubbles. These different models were critically reviewed and their limitations were unequivocally established. A hybrid model was also proposed predicting the scattering coefficient and the asymmetry factor by Lorenz–Mie theory while the absorption coefficient was expressed as the sum of absorption coefficients of the bubbles and the medium weighted by their respective volume fractions. Unlike previous models, the new hybrid model showed excellent agreement with rigorous Monte Carlo ray-tracing results based on geometric optics

in predicting the reflectance and transmittance for a wide range of bubble volume fractions, slab thicknesses, and absorption coefficients. In addition, a digital twin of a thick glass sample containing large number of gas bubbles was constructed using a microCT scan of the sample to extract bubble locations, size distribution, and volume fraction for input into the models. The predictions by the hybrid model were also in good agreement with the experimental measurements of the normal-hemispherical transmittance and reflectance in the spectral window between 0.4 and 3 μm when silica ranges from weakly absorbing to absorbing. These results highlight the adequacy and robustness of the hybrid model in rapidly simulating radiation transfer through a semi-transparent medium containing spherical bubbles with a wide range of bubble volume fraction and size distribution as well as different thicknesses and medium compositions. Additionally, the Dombrovsky model and the modified Lorenz–Mie theory predicted radiation transfer reasonably well only when the host medium was weakly absorbing. These results can be used to simulate or optimize radiation transfer in various applications in geoengineering, photoelectrochemistry, and materials manufacturing.

CRediT authorship contribution statement

Declaration of competing interest

The authors declare the following financial interests/personal relationships which may be considered as potential competing interests: Laurent Pilon is one of the Handling Associate Editors for the Journal of Quantitative Spectroscopy and Radiative Transfer.

Data availability

Data will be made available on request.

Acknowledgments

Appendix A. Supplementary data

Supplementary material related to this article can be found online at https://doi.org/10.1016/j.jqsrt.2023.108781.

References

[1] Pilon L, Viskanta R. Radiation characteristics of glass containing gas bubbles. J Am Ceram Soc 2003;86(8):1313–20.

[2] Dombrovsky L. The propagation of infrared radiation in a semitransparent liquid containing gas bubbles. High Temp 2004;42(1):133–9.

[3] Viskanta R, Mengüç MP. Radiative transfer in dispersed media. Appl Mech Rev 1989;42(9):241–59.

[4] Viskanta R. Review of three-dimensional mathematical modeling of glass melting. J Non-Cryst Solids 1994;177:347–62.

[5] Fedorov AG, Pilon L. Glass foams: formation, transport properties, and heat, mass, and radiation transfer. J Non-Cryst Solids 2002;311(2):154–73.

[6] Lee SW, Lim CH, Salleh EIB. Reflective thermal insulation systems in building: A review on radiant barrier and reflective insulation. Renew Sustain Energy Rev 2016;65:643–61.

[7] Dorfi AE, West AC, Esposito DV. Quantifying losses in photoelectrode performance due to single hydrogen bubbles. J Phys Chem C 2017;121(48):26587–97.

[8] Holmes-Gentle I, Bedoya-Lora F, Alhersh F, Hellgardt K. Optical losses at gas evolving photoelectrodes: implications for photoelectrochemical water splitting. J Phys Chem C 2018;123(1):17–28.

[9] Obata K, Abdi F. Bubble-induced convection stabilizes local pH during solar water splitting in neutral pH electrolytes. Sustain Energy Fuels 2021;5(15):3791–801.

[10] Kempler PA, Ifkovits ZP, Yu W, Carim AI, Lewis NS. Optical and electrochemical effects of H_2 and O_2 bubbles at upward-facing Si photoelectrodes. Energy Environ Sci 2021;14(1):414–23.

[11] Bhanawat A, Zhu K, Pilon L. How do bubbles affect light absorption in photoelectrodes for solar water splitting? Sustain Energy Fuels 2022;6(3):910–24.

[12] Bhanawat A, Pilon L. Light transfer through bubble-filled electrolyte for solar water splitting. Sustain Energy Fuels 2023;7(2):448–60.

[13] Berberoglu H, Yin J, Pilon L. Light transfer in bubble sparged photo-bioreactors for H_2 production and CO_2 mitigation. Int J Hydrogen Energy 2007;32(13):2273–85.

[14] Zhang D, Dechatiwongse P, Hellgardt K. Modelling light transmission, cyanobacterial growth kinetics and fluid dynamics in a laboratory scale multiphase photo-bioreactor for biological hydrogen production. Algal Res 2015;8:99–107.

[15] Zhang J-Y, Qi H, He Z-Z, Yu X-Y, Ruan L-M. Investigation of light transfer procedure and photobiological hydrogen production of microalgae in photobioreactors at different locations of China. Int J Hydrogen Energy 2017;42(31):19709–22.

[16] Evans J, Stride E, Edirisinghe M, Andrews D, Simons R. Can oceanic foams limit global warming? Clim Res 2010;42(2):155–60.

[17] Aziz A, Hailes HC, Ward JM, Evans JR. Long-term stabilization of reflective foams in sea water. RSC Adv 2014;4(95):53028–36.

[18] Kravitz B, Rasch PJ, Wang H, Robock A, Gabriel C, Boucher O, Cole JNS, Haywood J, Ji D, Jones A, Lenton A, Moore JC, Muri H, Niemeier U, Phipps S, Schmidt H, Watanabe S, Yang S, Yoon J-H. The climate effects of increasing ocean albedo: an idealized representation of solar geoengineering. Atmos Chem Phys 2018;18(17):13097–113.

[19] Dombrovsky LA, Kokhanovsky AA. Solar heating of ice sheets containing gas bubbles. J Quant Spectrosc Radiat Transfer 2020;250:106991.

[20] Kirillin GB, Shatwell T, Wen L. Ice-covered lakes of tibetan plateau as solar heat collectors. Geophys Res Lett 2021;48(14):e2021GL093429.

[21] Dombrovsky LA, Kokhanovsky AA. Solar heating of ice-covered lake and ice melting. J Quant Spectrosc Radiat Transfer 2023;294:108391.

[22] What is bubble glass?. 2022, https://glassdesigns.com/what-is-bubble-glass/. Accessed: 2022-12-07.

[23] Wikimedia commons images. 2022, https://commons.wikimedia.org/wiki/Category:Images. Accessed: 2022-12-07.

[24] Galy T, Huang D, Pilon L. Revisiting independent versus dependent scattering regimes in suspensions or aggregates of spherical particles. J Quant Spectrosc Radiat Transfer 2020;246:106924.

[25] Modest MF, Mazumder S. Radiative heat transfer. 4th ed.. New York, NY: Academic Press; 2021.

[26] Howell JR, Mengüç MP, Daun K, Siegel R. Thermal radiation heat transfer. 7th ed.. Boca Raton, FL: CRC Press; 2020.

[27] Zhu K, Huang Y, Pruvost J, Legrand J, Pilon L. Transmittance of transparent windows with non-absorbing cap-shaped droplets condensed on their backside. J Quant Spectrosc Radiat Transfer 2017;194:98–107.

[28] Zhu K, Pilon L. Transmittance of semitransparent windows with absorbing cap-shaped droplets condensed on their backside. J Quant Spectrosc Radiat Transfer 2017;201:53–63.

[29] Mundy W, Roux J, Smith A. Mie scattering by spheres in an absorbing medium. J Opt Soc Amer 1974;64(12):1593–7.

[30] Chylek P. Light scattering by small particles in an absorbing medium. J Opt Soc Amer 1977;67(4):561–3.

[31] Sudiarta IW, Chylek P. Mie scattering efficiency of a large spherical particle embedded in an absorbing medium. J Quant Spectrosc Radiat Transfer 2001;70(4–6):709–14.

[32] Fu Q, Sun W. Mie theory for light scattering by a spherical particle in an absorbing medium. Appl Opt 2001;40(9):1354–61.

[33] Sun W, Loeb NG, Fu Q. Light scattering by coated sphere immersed in absorbing medium: a comparison between the FDTD and analytic solutions. J Quant Spectrosc Radiat Transfer 2004;83(3–4):483–92.

[34] Fedorov A, Viskanta R. Radiative transfer in a semitransparent glass foam blanket. Phys Chem Glasses 2000;41(3):127–35.

[35] Fedorov AG, Viskanta R. Radiation characteristics of glass foams. J Am Ceram Soc 2000;83(11):2769–76.

[36] Dombrovsky L, Randrianalisoa J, Baillis D, Pilon L. Use of Mie theory to analyze experimental data to identify infrared properties of fused quartz containing bubbles. Appl Opt 2005;44(33):7021–31.

[37] Dombrovsky L, Baillis D. Thermal radiation in disperse systems: An engineering approach. New York, NY: Begell House; 2010.

[38] Yang P, Gao B-C, Wiscombe WJ, Mishchenko MI, Platnick SE, Huang H-L, Baum BA, Hu YX, Winker DM, Tsay S-C, Park SK. Inherent and apparent scattering properties of coated or uncoated spheres embedded in an absorbing host medium. Appl Opt 2002;41(15):2740–59.

[39] Wu L, Yang H, Li X, Yang B, Li G. Scattering by large bubbles: Comparisons between geometrical-optics theory and debye series. J Quant Spectrosc Radiat Transfer 2007;108(1):54–64.

[40] Van de Hulst HC. Light scattering by small particles. Mineola, NY: Dover Publications; 1981.

[41] Orchard SE. Reflection and transmission of light by diffusing suspensions. J Opt Soc Amer 1969;59(12):1584–97.

[42] Egan WG, Hilgeman TW. Optical properties of inhomogeneous materials: Applications to geology, astronomy, chemistry and engineering. New York, NY: Academic Press; 1979.

[43] Davison B, Sykes J. Neutron transport theory. London: Oxford University Press; 1957.

[44] McKellar BH, Box MA. The scaling group of the radiative transfer equation. J Atmos Sci 1981;38(5):1063–8.

[45] Etherden N, Tesfamichael T, Niklasson G, Wäckelgård E. A theoretical feasibility study of pigments for thickness-sensitive spectrally selective paints. J Phys D: Appl Phys 2004;37(7):1115.

[46] Yalçın RA, Blandre E, Joulain K, Drévillon J. Colored radiative cooling coatings with nanoparticles. ACS Photonics 2020;7(5):1312–22.

[47] Yalçın RA. Monte Carlo mie scattering code. 2020, https://github.com/refetaliyalcin/monte-carlo-mie-scattering, [Online; accessed 18-January-2022].

[48] Baillis D, Pilon L, Randrianalisoa H, Gomez R, Viskanta R. Measurements of radiation characteristics of fused quartz containing bubbles. J Opt Soc Amer A 2004;21(1):149–59.

[49] Kitamura R, Pilon L, Jonasz M. Optical constants of silica glass from extreme ultraviolet to far infrared at near room temperature. Appl Opt 2007;46(33):8118–33.

[50] Malitson IH. Interspecimen comparison of the refractive index of fused silica. J Opt Soc Amer 1965;55(10):1205–9.

[51] Loening AM, Gambhir SS. AMIDE: a free software tool for multimodality medical image analysis. Mol Imaging 2003;2(3):15353500200303133.